Construction and Building Materials 226 (2019) 712–720

Contents lists available at ScienceDirect

Construction and Building Materials

journal homepage: www.elsevier.com/locate/conbuildmat

Correlation between pore characteristics and tensile bond strength of additive manufactured mortar using X-ray computed tomography

Hojae Lee [a,b], Jang-Ho Jay Kim [b,*], Jae-Heum Moon [a], Won-Woo Kim [a], Eun-A Seo [a]

[a] Korea Institute of Civil Engineering and Building Technology, Daehwa-Dong, Goyang-Si, Gyeonggi-Do 10223, South Korea
[b] School of Civil and Environmental Engineering, Yonsei University, Shinchon-dong, Seodaemun-gu, Seoul 03722, South Korea

HIGHLIGHTS

- Pore distribution in the interlayer analyzed using X-ray Computed Tomography.
- Relationship between pore fraction and position of tensile bond fracture determined.
- Tensile bond strength of 6.27% of compressive strength obtained.
- Weakest layer occurred when tensile stress is perpendicular to printing direction.

ARTICLE INFO

Article history:
Received 23 November 2018
Received in revised form 15 May 2019
Accepted 17 July 2019

Keywords:
3D printing
Additive manufacturing
Interlayer
Pore fraction
X-ray CT
Tensile bond strength

ABSTRACT

Recently, researches on additive manufacturing (AM) method have been actively carried out as the latest technique for building concrete structures in the construction field. It is known that the additive manufacturing method, also called 3D printing technique, is a method of constructing a structure by printing layers, and the adhesion strength in the interlayer between the layers plays a dominant role in the performance of the structure. In this study, we focused on the formation of interlayer of concrete structure built using additive manufacturing method. In this study, the position of the interlayer was analyzed using the computed tomography (CT) method and the correlation between porosity and tensile bond strength in the analyzed interlayer was tried. As a result of the CT analysis of 13 specimens extracted from the printed specimens, it was confirmed that the porosity was formed high in the interlayer. The porosity of the interlayer was at least 2.15% and 6.66% higher than the average porosity. After analyzing the porosity by CT, the tensile bond strength of the specimens was measured to confirm the tensile bond strength and location of the fracture surface. Tensile bond strengths were 2.58–3.77 MPa with an average of 2.80 MPa using 10 specimens. It was confirmed that all of the fracture surfaces occurred along the interlayer. It was confirmed that there was no correlation between the tensile bond strength and porosity of the test specimens used in this study. Six of the ten specimens failed in the other interlayer, but four specimens failed in the interlayer with the highest porosity. As a result of analysis of the fracture surfaces of six specimens without fracture at the highest porosity, the porosity at the fracture surface was 5.73–9.18%, which was higher by 0.6–3.3% than the average porosity. However, defects occurred during layer output were confirmed from the failure of six specimens. Through this study, we confirmed that the interlayer is the weakest when tensile stress is applied in the perpendicular direction of printing, and that it is necessary to review the defects when applying the printing method.

1. Introduction

Recently, concrete additive manufacturing (AM) using a 3D printing technique has been developed actively because it is a free-formed construction method that can be used for building irregular concrete structures. The traditional method of concrete construction involves pouring concrete into forms. Accordingly, when new concrete is placed in contact with hardened concrete, the tensile bond strength between the concrete interfaces has to be considered to prevent cold joints. On the other hand, concrete AM requires that the tensile bond strength of every interlayer be examined because the performance of a structure constructed by the AM method mainly depends on the bond strength of the

* Corresponding author.
E-mail addresses: h.lee@kict.re.kr (H. Lee), jjhkim@yonsei.ac.kr (J.-H.J Kim), mjh4190@kict.re.kr (J.-H. Moon), kimwonwoo@kict.re.kr (W.-W. Kim), sea0524@kict.re.kr (Eun-A Seo).

https://doi.org/10.1016/j.conbuildmat.2019.07.161
0950-0618/

interlayer. In particular, as a viscous concrete mixture is applied to each interlayer to ensure the buildability of the material, pores or voids are very likely to be entrapped in an interlayer, which influences the strength of the concrete.

Typically, because the pore structure of concrete has a great effect on its physical and mechanical properties, many studies have been conducted to quantitatively evaluate the pore structure of the material in various fields [1–3]. Pore size and pore size distribution (PSD) are essential factors for morphologically characterizing the pore structure within concrete. Existing studies on the pore structure of concrete have focused mainly on the impacts of porosity and permeability on durability by using methods, such as mercury intrusion porosimetry (MIP) [4–6]. In most cases, pore structure is evaluated by indirect measurements based on the analytic method of injecting fluids, such as mercury, into the pores. However, this method can hardly estimate PSD and usually results in large measurement errors.

Regarding the correlation between the pore structure and mechanical properties of concrete, Chen et al. [7] estimated the pore volume by measuring the absorption of concrete and also evaluated relationships with pore volume and mechanical properties, thus obtaining information about the mechanical properties (compressive strength and splitting tensile strength). Zhao et al. [8] used MIP to evaluate pore structure and determine how compressive strength is affected by pore structure. Unlike the case of capillary pores, it is difficult to evaluate entrapped pores quantitatively because the injection of a fluid under pressure has limitations for measurement. However, X-ray computed tomography (CT) has recently been used to evaluate the internal pore structure of concrete. To assess durability, Darma et al. [9] examined internal pores and diffusion through cracks by X-ray CT. For fractures, Wenyuan et al. [10] analyzed pores, aggregates, and hydrates using X-ray CT and developed a meso-scale fracture model. Wenyuan et al. also utilized X-ray CT to estimate pore distributions according to the deposition shapes of concrete, and identify the relationship between pore distribution and tensile strength.

X-ray CT is a technique for visualizing the internal structure of a material by utilizing the X-ray attenuation characteristics of the material. This technique was first developed for medical purposes in the 1970s but began to be applied for industrial purposes from the 1980s. X-ray CT equipment transmits X-rays from a generator through a material and measures the amount of X-ray attenuation by using a device called a detector. The CT data thus obtained are reconstructed and finally transformed into slice digital data. The digital data are visualized as 3D images using software or can be utilized for various analyses [11]. Since the X-ray CT-based analysis is a nondestructive process; the same specimen can be used for additional experiments after the analysis. Additionally, if the analysis process is well established, less time and effort is required than that required for other experimental methods. X-ray CT equipment has been applied mainly to analyze the density variations and pore volumes of materials. However, as the equipment and analysis techniques have developed, there have been many attempts to apply X-ray CT to the analysis of failure behaviors or numerical mechanical behaviors of materials [12,13]. From the pore structure characteristics of the interlayer that occurs during AM, this study estimated pore size distributions by X-ray CT. Then, the impact of interlayer quality on the tensile bond strength between layers was evaluated by using the obtained pore size distributions.

To evaluate the tensile bond strength, which was the goal of this study, existing experimental methods and results were reviewed. Many studies have attempted to evaluate the mechanical properties of AM concrete (compressive strength, flexural strength, tensile bond strength, etc.) by applying conventional testing methods. AM specimens used for evaluating mechanical performance have been printed by either of the two following methods. In the first method, a single interface is created for testing [4,5]. This method can minimize the defects that occur due to multiple interfaces during an experiment using multi layers. In the second method, a printer is used for continuous printing, and the many layers thus printed are cut to the size of a specimen [6–9]. In this case, many interfaces are generated within a specimen, which may increase the possibility of a defect between the interlayers. However, the evaluation of the specimen can closely reflect the mechanical performance of the real printed concrete.

There are three methods for evaluating the bond strength of the interlayers. In the first method, the tensile bond strength between layers is evaluated by applying a tensile load perpendicular to the deposition direction [14–17]. In the second method, the sliding capacity between the layers is evaluated [18,19] by applying two loads in opposite directions to a layer parallel (longitudinal or lateral) to the deposition direction. In the third method, the splitting tensile strength is evaluated by generating a compressive load in the direction parallel to the interlayer (splitting method) [20]. In the present study attempts to evaluate the effects of pore volume and structure between layers on tensile bond strength by examining the internal state of AM concrete. To achieve this goal, multilayer specimens were printed, and their tensile bond strengths were evaluated by the direct tension method. This study printed multi-layer specimens because specimens with multiple interlayers, which are produced by AM, might reflect the true performance of a real structure. In addition, before the tensile bond strength test, CT analysis was conducted to obtain interlayer shape, pore structure, and defects of each specimen, which was utilized to analyze the correlation to a section having a real fracture.

2. Specimen preparation and experimental method

2.1. Materials

For mix proportion, three types of cementitious materials were used: OPC (ordinary Portland cement), FA (Fly Ash), SF (Silica fume). Type I OPC with specific gravity of 3.13 g/cm^3 was used as a major binder in this study. The initial and final setting times of OPC were calculated in the laboratory and the values are determined as 263 min and 360 min. Class C FA with specific gravity of 2.25 g/cm^3 was used. Loss on ignition of FA was calculated as 2.5%. The non-densified SF having a SiO_2 content of 91.3% was also used. Percent retained on 45-μm (No. 325) of SF was 4.4%. The sand with 0.16–0.2 mm size was selected considering the maximum grain size capacity of the pump. The specific gravity of the sand was measured to be 2.59 g/cm^3. Polycarboxylic acid high performance water reducing agent (HWRA) and cellulose viscosity agent were used as the admixture.

2.2. Determination of mix proportion for printing

As shown in Fig. 1, the extrudability and buildability of the cement based composite mortar for the experiment were verified using a 3D printing device before printing the specimens. After the materials for printing the specimens were mixed, fluidity and rheological properties (yield stress and plastic viscosity) were evaluated. Extrudability and buildability were tested to determine an appropriate mix proportion for the printing test using mono-pump type extruder (see Fig. 1).

For mix proportion (Table 1), the water-binder ratio was determined to be 28% based on the results of previous studies. Also, binder replacement ratio is selected based on the same research results [16]. In this study, factors that affect tensile bond strength due to using multiple material usage are minimized. In order to prevent

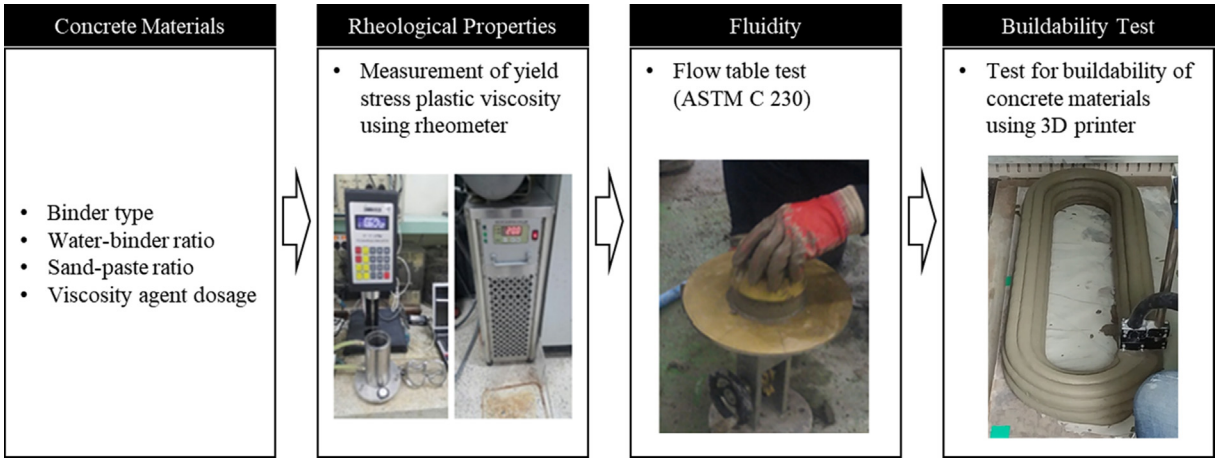

Fig. 1. Experimental process of determining the suitable mix proportion.

Table 1
Mix proportion for printing.

W/B (%)	Binder contents ratio (%)			Unit weight (kg/m^3)						Note
	OPC	FA	SF	Water	OPC	FA	SF	Sand	HWRA	Viscosity agent
28	70	20	10	232	580	166	83	1146	8.29	0–1.0%

material changes that can occur by using various materials, the specimens are manufactured using one mix proportion type.

The mortar fluidity was evaluated by flow table test according to ASTM C 1437 method. As shown in Table 2, the flow performance was evaluated by increasing the viscosity agent to 0%–1.0% in increments of 0.2% in 5 steps by binder weight to determine the mix proportion with flow performance suitable for printing.

The extruding test was carried out using a mono-pump type extruder with a flow table test simultaneously. The specifications of the mono-pump type extruder used in this research were as shown in Table 3. As a result of the both tests, the range of flow table test result which can be extruded and additive manufactured was 160–170 mm by flow table test and the mix proportion was determined by applying viscosity agent at 0.4%. Applied mix proportion in this study had the following rheological properties: rheological yield stress of 670 Pa and plastic viscosity of 141 Pa·s.

A setting time test according to ASTM C 403 method was performed to determine the possibility of mortar setting during the printing process. As a result of the setting time test, the initial setting time was 424 min and the final setting time was 602 min.

2.3. Preparation of specimens

The mix proportion obtained by verifying the extrudability and buildability of the mortar was applied to print specimens ($50 \times 50 \times 50$ mm) for testing compressive strength by using a 3D printer and AM mortar specimens for collecting core. To see the relationship between the layers and tensile bond strength, the AM mortar specimens were printed by utilizing a mono-pump type extruder. Once the materials were mixed, the layers were continuously printed to minimize the decrease of tensile bond strength at each interlayer due to the time gap. To print an AM mortar for coring, printing speed and bead height were determined as following: printing speed 70 sec/layer, height 15 mm/layer. After printing, the AM mortar was cured for 28 days, as shown in Fig. 2, following which 13 specimens with a length of 60 mm each were collected using a 45 mm core drill for capturing X-ray CT images of pore fraction.

Table 2
Flow table test results according to viscosity agent usage.

Viscosity agent (%)	0.0	0.2	0.4	0.6	0.8	1.0
Results of flow table test (mm)	218	180	165	158	143	133

Table 3
Specifications of the mono-pump type extruder for printing.

Working pressure (bar)	Conveying capacity (liter/min)	Motor capacity (kW – rpm)	Maximum grain size (mm)
20	9	1.9 – 170	3

2.4. X-ray CT image acquisition and analysis

X-ray CT is a technique based on the principle that the number of X-ray photons absorbed or scattered as X-rays pass through matter is proportional to the density and atomic number of the matter. The X-ray intensity (I) is expressed by the linear attenuation coefficient (μ), which has the unit of cm^{-1}, and can be defined by the following equation.

$$I_x = I_0 e^{-\mu x} \quad (1)$$

where I_x is the intensity at the depth of x cm, I_0 is the original intensity, and μ is the linear attenuation coefficient.

For X-ray CT analysis, industrial X-ray CT equipment from the KICT(Korea Institute of Civil Engineering and Building Technology) was used with conditions of 200 microamps at 120 kV, 1 s capturing time and 166.8 mm of SOD (source object detection – distance from X-ray tube to sample).

Images were extracted at a height of 50 mm by excluding the upper and bottom parts of each 60-mm-long specimen. After the images were analyzed and tensile strength was measured, a reference point was marked on each specimen to evaluate fracture surfaces comparatively. The images were analyzed based on this reference point.

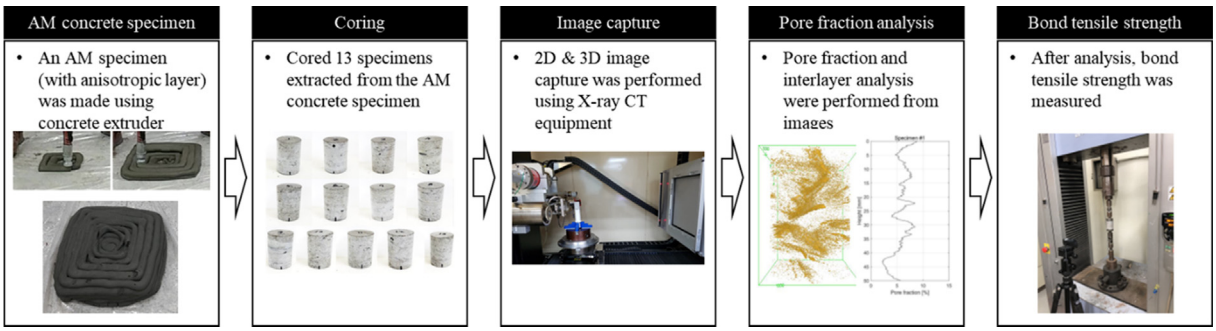

Fig. 2. X-ray CT image acquisition and measurement of tensile bond strength after printing of AM mortar specimens.

Binarization is the most important process for analyzing the pore structure of a material from CT images. It involves reconfiguring the intensity values of each pixel distributed in a CT image into 0 or 1. For this process, setting a threshold is essential. Many theoretical suggestions for efficiently setting thresholds have been proposed [21]. In general, to extract a pore with a lower CT number, set a constant threshold value and select a value less than that threshold. Therefore, the value of the pore volume, or positivity, changes depending on the value of the threshold determined. In this study, the threshold value was applied to 180 CT number in an 8-bit image and a pixel with a CT number smaller than that value was determined as a pore. An identical threshold value was applied to all 13 specimens, and pores were extracted from the internal structures of the specimens. To evaluate the interlayers, images were acquired every 70 μm from the top of each specimen, resulting in a total of 750 CT images from each specimen. Through the image analysis, pore fractions were calculated at each depth.

2.5. Tensile bond strength and compressive strength

After the X-ray CT analysis, the circular specimens with a diameter of 45 mm and length of 60 mm were tested for tensile strength in accordance with BS EN 14488-4:2005. For the tensile strength test, dollies with a diameter of 50 mm and thickness of 25 mm that can be mounted on a device. After 28 days curing, dollies were attached to both ends of each specimen using a high-strength epoxy glue and the glue was cured for 1 day. The tensile strength was measured with displacement control at a loading speed of 0.3 mm/min. Test was performed for all 13 specimens, and the result was compared with the pore analysis result. The cubic specimens (50 × 50 × 50 mm), which were printed along with the AM mortar specimens, were used to measure compressive strength at 1, 3, 7, and 28 days after specimen printing. Three specimens were used to measure compressive strength at each age and the mean values of each age were adopted. The compressive strength was measured at a loading speed of 0.3 MPa/s.

3. Results

3.1. Compressive strength and tensile bond strength

The compressive strengths at 1, 3, 7, and 28 days were 8.37, 22.16, 39.81, and 44.58 MPa, respectively, as shown in Fig. 3. When the result of 28 days was used as a baseline, the compressive strength had developed to 50% and 90% at 3 days and 7 days, respectively.

Tensile bond strength was evaluated using all 13 specimens. Fig. 4 illustrates the result of the tensile bond strength test, which is indicated by the box-and-whisker plot to the right of Fig. 4. Among the 13 specimens, specimen nos. 7, 11, and 12 showed

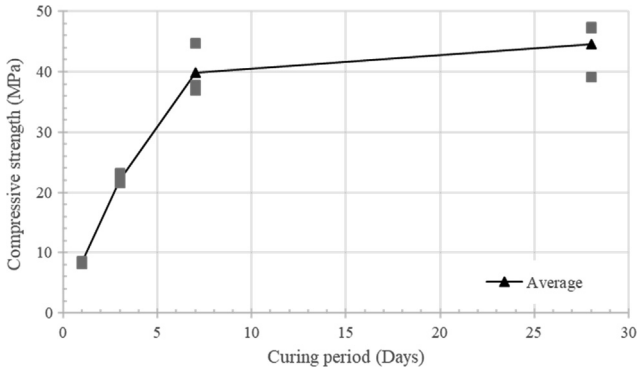

Fig. 3. Compressive strengths at 1, 3, 7, and 28 days.

destruction of the epoxy glue applied between the dollies and each specimen. Accordingly, the box-and-whisker plot includes the results of only 10 specimens, excluding the 3 with damaged glue.

As illustrated in Fig. 4, the maximum tensile bond strength was 3.77 MPa, and the minimum and average tensile bond strengths were 2.58 and 2.80 MPa (or 3.07 MPa if the outlier is excluded), respectively. The tensile bond strength is typically predicted to be around 10% of the compressive strength. However, in this experiment, the tensile bond strength was less than 7% (about 6.27%) of the compressive strength.

A similar trend was also observed in one of the aforementioned previous studies [16]. Fig. 5 reinterprets the result of that study. The compressive strength was 107 MPa (mold casting) and the tensile bond strengths were 3.0 (direct) and 2.3 MPa (printing time gap of 0–15 min). In this case, the tensile bond strength was about 2–3% of the compressive strength.

This difference in the percentage of tensile bond strength between this study and the previous study is mainly attributable to the printing quality. According to the number of voids after printing, printing quality is classified into poor and good categories; the printing quality is better when there are fewer voids. However, the existing studies on 3D printing have not evaluated the direct relationship between the number of voids and tensile bond strength. Moreover, the previous study referred to above used a specimen with a diameter of 58 mm and height of 120 mm to measure tensile bond strength. This difference in specimen size seems to be one of the reasons why the tensile bond strength was comparatively lower in comparison to the present study. Because it is difficult to constantly maintain the tensile bond strength of every interlayer, if any layer has a defect, the tensile bond strength will naturally decrease. Thus, the tensile bond strength is very likely to decrease with increase in the height of the specimen (more layers). To analyze the correlations

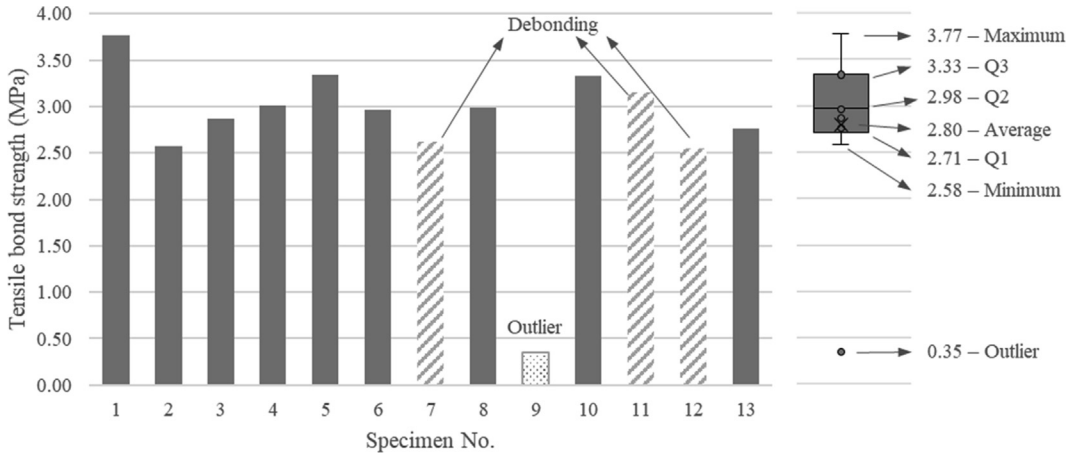

Fig. 4. Tensile strength of cored specimens at 28 days.

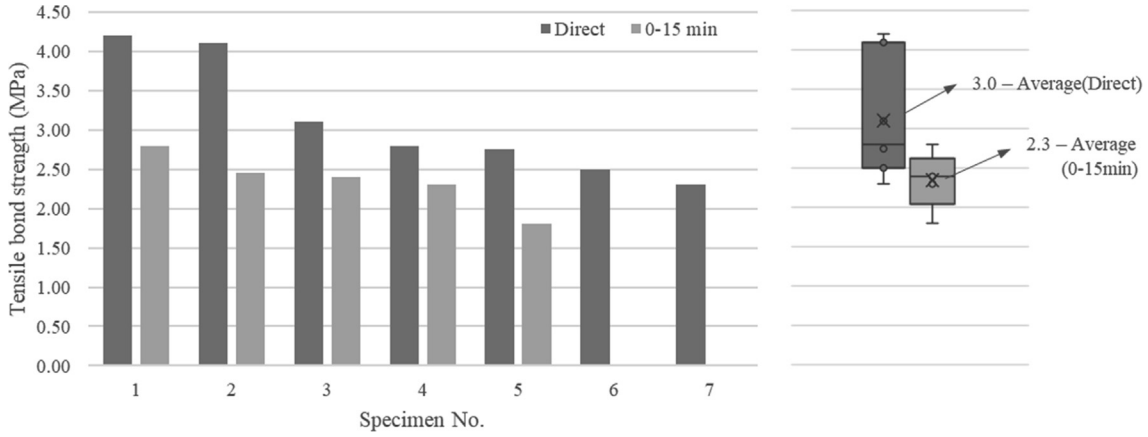

Fig. 5. Reinterpretation of the test result from a previous study [16].

among printing quality, defects, and tensile bond strength, in this study examined pore (void) fractions and defects on fracture surfaces.

3.2. Pore fraction analysis from CT images

Pore fraction was analyzed according to the height of the specimen using the X-ray CT images. Fig. 6 show that there were interlayers at the pore fraction peaks. The existence of an interlayer in the perpendicular direction could hardly be judged based on the analysis of the parallel direction. Thus, analysis of the pore fraction in the perpendicular direction is essential.

From the CT images, specimen had at least one interlayer formed by two layers deposited in the parallel direction because the nozzle diameter was 25 mm. In addition, because the height of a layer was 15 mm, 4 or more layers were deposited in the perpendicular direction, so that 3–4 interlayers were generated. When the pore fraction was analyzed using X-ray CT images, 10 out of 13 specimens exhibited at least 3 interlayers. In other words, because 3 specimens were excluded from the X-ray CT analysis, almost all of the specimens had 3 or more interlayers. On the other hand, specimens 7, 10, and 12 exhibited some traces of interlayer in CT images but no remarkable visible pores. This was because the quality of the mortar in the interlayers was improved by sufficient bonding during the AM.

3.3. Correlation between pore fraction and tensile bond strength

Fig. 7 illustrates the comparison of the pore fractions obtained by the CT image analysis of specimens with the images of the tensile fractured specimens. Each of the highest pore fractions was marked by a blue star and each real fracture surface was distinguished by an orange star. As illustrated in Fig. 7, the fractures occurred in areas of high pore intensity. However, only 4 out of 10 specimens, showed a fracture occurring along the surface with the highest pore intensity, indicating that the probability was not especially high.

As shown in Fig. 8, the characteristics of the fracture surface were examined according to the pore fraction by using perpendicular images. Small pores were observed in the printed layers. However, these pores were very small, located at the bottom of the image, and did not significantly affect the total area. Accordingly, the parallel images were analyzed for the surface with the highest pore fraction and the real fracture surface to clarify the reason for the discrepancy.

As shown in Fig. 9, the parallel CT image, which was evaluated to have the highest pore fraction, actually had many pores (upper left). On the other hand, in the case of the real fracture surface (bottom left), the measured pore fraction was relatively low.

Fracture occurred more easily at the real fracture surface because the pores of the interlayer led to a defect influencing the load delivery. These results were also observed in specimens 1, 3,

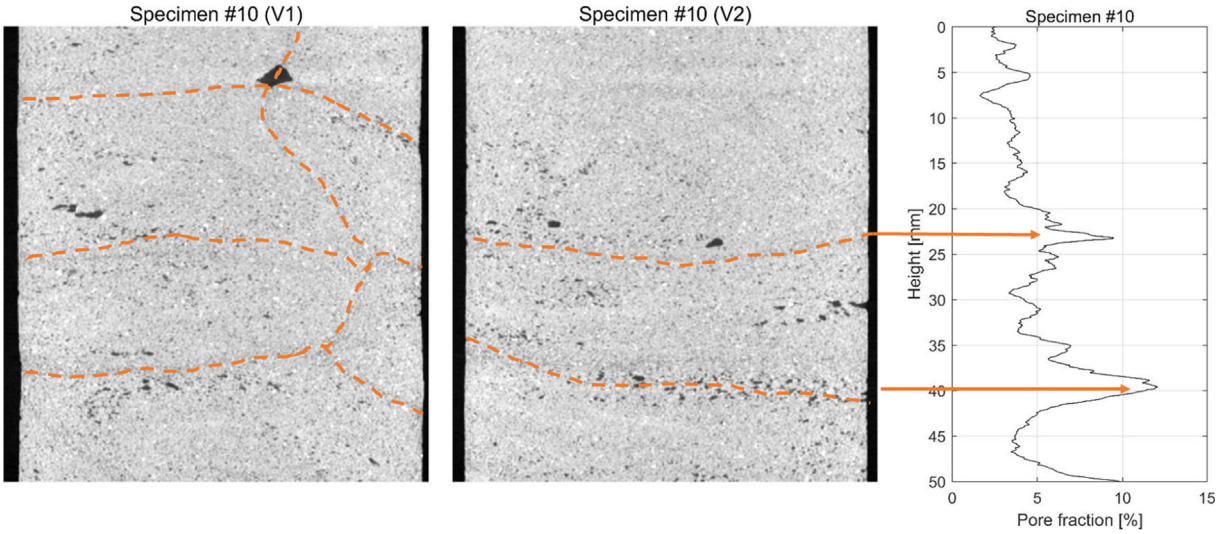

Fig. 6. Relationship between perpendicular image and pore fraction by using X-ray CT of a cored specimen.

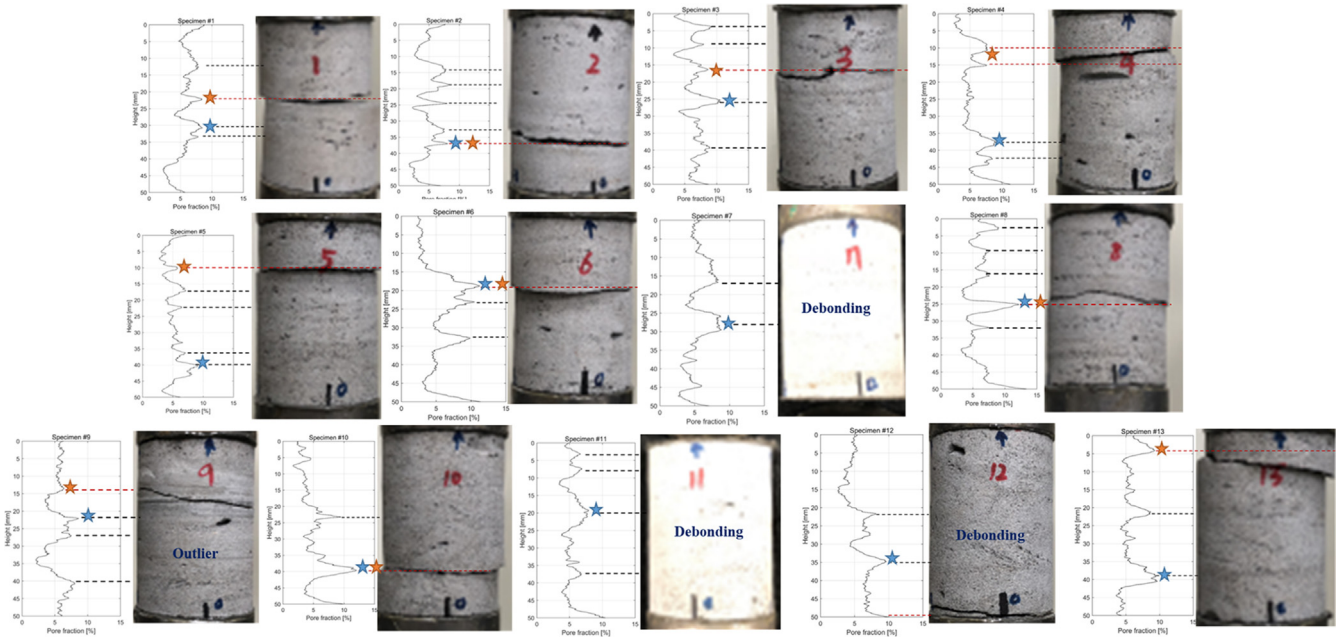

Fig. 7. Correlation between pore fraction and real fracture surfaces.

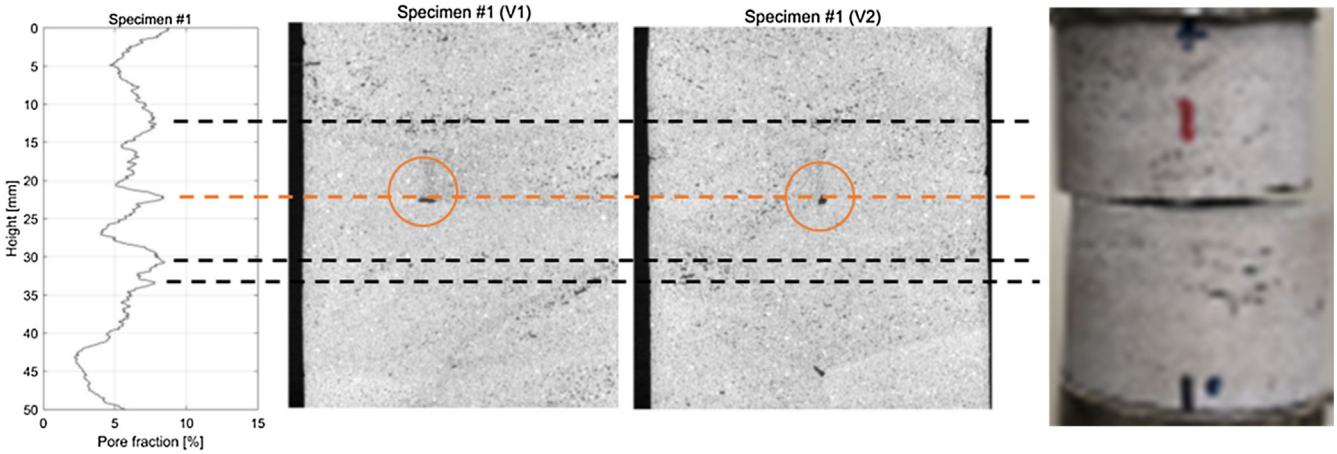

Fig. 8. Pore fraction of real fracture surface and the analysis of perpendicular images.

4, 5, 9, and 13, all of which showed a discrepancy between the surface with the highest pore fraction and the real fracture surface (Fig. 10). On the other hand, as shown in Fig. 11, the CT images of the specimens 2, 6, 8, and 10 showed that the porosity was relatively high compared to Fig. 10.

Fig. 12 illustrated the correlation between pore fraction (mean value and the value at the fracture surface) and tensile bond strength. As shown in Fig. 12, the tensile bond strength is in the range of 2.5–3.9 MPa with little correlation with the mean pore fraction. The pore fraction at the fracture surface showed a

Fig. 9. Parallel images along with fracture surface images (No. 1).

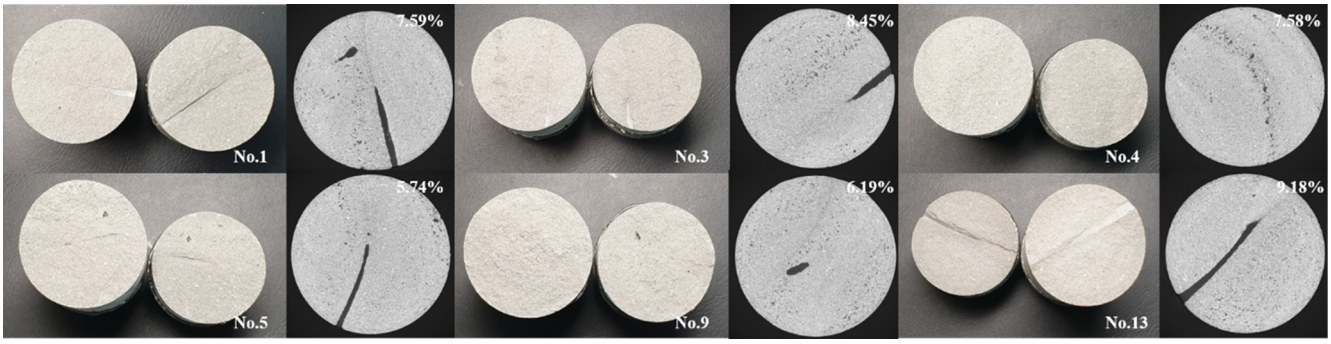

Fig. 10. Images of specimens and CT images at fracture surfaces (No. 1, 3, 4, 5, 9 and 13).

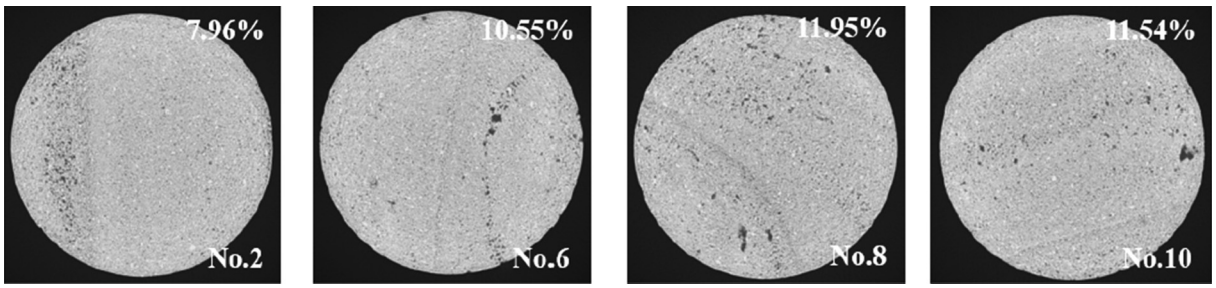

Fig. 11. Images of specimens and CT images at fracture surfaces (No. 2, 6, 8 and 10).

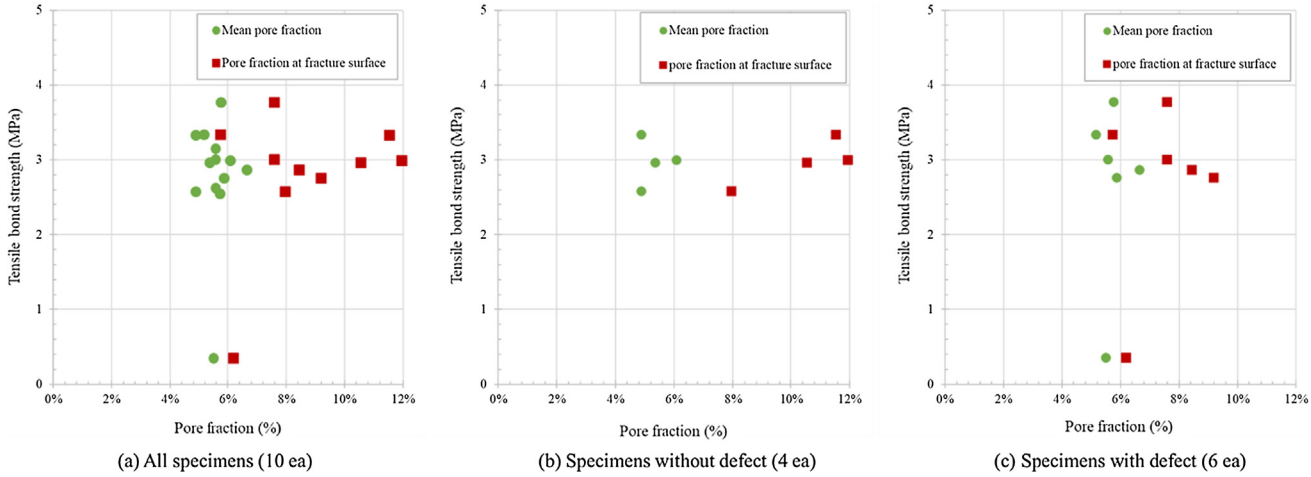

Fig. 12. Relationship between pore fractions and tensile bond strength.

difference of at least 0.6% and a maximum of 5.7% over the mean pore fraction. However, the pore fraction at the fracture surface was not significantly related to the tensile bond strength.

When the AM method was used to print the mortar, the pore volume was concentrated along the interfaces, as observed in almost every specimen. However, it was confirmed that the strength of the mortar was not directly affected by the mean pore fraction and printing quality of the mortar.

4. Conclusion

This study analyzed the pore size distribution in the interlayer, relationship between the pores and tensile strength, and tensile fracture in the interlayer using mortar specimens produced by AM. When the specimens were printed, the materials were mixed only once and then the whole process from extrusion to print was conducted without interruption. This was done to minimize the error rate due to material change and mixing time, thereby minimizing the impact of material properties on tensile bond strength. Accordingly, the pores of the interlayer could be considered the only influential factor for tensile bond strength.

Based on the correlation analysis between the pore fraction obtained by X-ray CT analysis and the result of the tensile strength test, this study arrived at the following conclusions.

1) At 28 days, the average compressive strength was 44.58 MPa and the average tensile strength was 2.80 MPa (or 3.07 MPa if the outlier is excluded). The tensile strength was approximately 6.27% of the compressive strength. This result is below the typical result of 10%. One previous study demonstrated a similar but lower trend. The reason for this phenomenon seemed to be that the printing quality of the interlayers becomes more influential with the increase in the number of layers.
2) Interlayers were observed at heights where the pore fraction showed a drastic increase of intensity. However, some specimens showed a relatively smaller number of pores despite the interlayers because the printing quality was good. Therefore, if the printing quality can be controlled, the tensile bond strength of the interlayer can be sufficiently improved, thereby making integrated behavior feasible.
3) The total pore volume of the specimen did not affect the tensile strength of the mortar in this study. Additionally, the pore volume of the interlayer did not directly affect the failure of the mortar. Thus, even if the pore volume is low, a pore may spread and develop into a defect that can be influential for fracture formation.
4) Through this study, it was confirmed that, in the case of printed mortar made by the AM method, it is possible to evaluate the porosity of the interlayer which can not be visually evaluated by the CT method. It was confirmed that the porosity was distinctively high in the interlayer, and that the defect also occurred in the interlayer.
5) Although the types of materials and the types of output methods discussed in this study are not various, it is not enough to give a general opinion on the effect of the defect on the tensile bond strength. However, the factors affecting the tensile bond strength in the interlayer It seems to have presented one direction.

Declaration of Competing Interest

The authors declare no conflict of interest.

Acknowledgement

This research was supported by a grant (17AUDP-B121595-02) from Urban Architecture Research Program funded by Ministry of Land, Infrastructure and Transport of Korean government.

References

[1] D. Winslow, D. Liu, The pore structure of paste in concrete, Cem. Concr. Res. 20 (1990) 227–235, https://doi.org/10.1016/0008-8846(90)90075-9.
[2] C. Lian, Y. Zhuge, S. Beecham, The relationship between porosity and strength for porous concrete, Constr. Build. Mater. 25 (2011) 4294–4298, https://doi.org/10.1016/j.conbuildmat.2011.05.005.
[3] D. Li, Z. Li, C. Lv, G. Zhand, Y. Yin, A predictive model of the effective tensile and compressive strengths of concrete considering porosity and pore size, Constr. Build. Mater. 170 (2018) 520–526, https://doi.org/10.1016/j.conbuildmat.2018.03.028.
[4] J. Zhang, F. Bian, Y. Zhang, Z. Fang, C. Fu, J. Guo, Effect of pore structures on gas permeability and chloride diffusivity of concrete, Constr. Build. Mater. 163 (2018) 402–413, https://doi.org/10.1016/j.conbuildmat.2017.12.111.
[5] B. Li, J. Mao, T. Nawa, T. Han, Mesoscopic damage model of concrete subjected to freeze-thaw cycles using mercury intrusion porosimetry and differential scanning calorimetry (MIP-DSC), Constr. Build. Mater. 147 (2017) 79–90, https://doi.org/10.1016/j.conbuildmat.2017.04.136.
[6] S.-W. Cho, Using mercury intrusion porosimetry to study the interfacial properties of cement-based materials, J. Mar. Sci. Technol. 20 (2012) 269–273.
[7] X. Chen, S. Wu, J. Zhou, Influence of porosity on compressive and tensile strength of cement mortar, Constr. Build. Mater. 40 (2013) 869–874, https://doi.org/10.1016/j.conbuildmat.2012.11.072.

[8] H. Zhao, Q. Xiao, D. Huang, S. Zhang, Influence of pore structure on compressive strength of cement mortar, Sci. World J. 247058 (2014), https://doi.org/10.1155/2014/247058.
[9] I.S. Darma, T. Sugiyama, M.A.B. Promentilla, Application of x-ray CT to study diffusivity in cracked concrete through the observation of tracer transport, J. Adv. Concr. Technol. 11 (2013) 266–281, https://doi.org/10.3151/jact.11.266.
[10] W. Ren, Z. Yang, R. Sharma, Ch. Zhang, P.J. Withers, Two-dimensional X-ray CT image based meso-scale fracture modelling of concrete, Eng. Fract. Mech. 133 (2015) 24–39, https://doi.org/10.1016/j.engfracmech.2014.10.016.
[11] H. Taud, R. Martinez-Angeles, J.F. Parrot, L. Hernandez-Escobedo, Porosity estimation method by X-ray computed tomography, J. Petrol. Sci. Eng. 47 (2005) 209–217, https://doi.org/10.1016/j.petrol.2005.03.009.
[12] A. du Plessis, T. Seifert, G. Booysen, J. Els, Microfocus x-ray computed tomography (CT) analysis of laser sintered parts, S. Afr. J. Ind. Eng. 25 (2014) (2014) 2224–7890.
[13] G.L. Balázs, É. Lublóy, T. Földes, Evaluation of concrete elements with X-ray computed tomography, J. Mater. Civ. Eng. 30 (2018).
[14] J.G. Sanjayan, B. Nematollahi, M. Xia, T. Marchment, Effect of surface moisture on inter-layer strength of 3D printed concrete, Constr. Build. Mater. 172 (2018) 468–475, https://doi.org/10.1016/j.conbuildmat.2018.03.232.
[15] B. Panda, S.C. Paul, N.A.N. Mohamed, Y.W.D. Tay, M.J. Tan, Measurement of tensile bond strength of 3D printed geopolymer mortar, Measurement 113 (2018) 108–116, https://doi.org/10.1016/j.measurement.2017.08.051.
[16] T.T. Le, S.A. Austin, S. Lim, R.A. Buswell, R. Law, A.G.F. Gibb, T. Thorpe, Hardened properties of high-performance printing concrete, Cem. Concr. Res. 42 (2012) 558–566, https://doi.org/10.1016/j.cemconres.2011.12.003.
[17] P. Shakor, J. Sanjayan, A. Nazari, S. Nejadi, Modified 3D printed powder to cement-based material and mechanical properties of cement scaffold used in 3D printing, Constr. Build. Mater. 138 (2017) 398–409, https://doi.org/10.1016/j.conbuildmat.2017.02.037.
[18] P. Feng, X. Meng, J.-F. Chen, L. Ye, Mechanical properties of structures 3D printed with cementitious powders, Constr. Build. Mater. 93 (2015) 486–497, https://doi.org/10.1016/j.conbuildmat.2015.05.132.
[19] B. Panda, S.C. Paul, M.J. Tan, Anisotropic mechanical performance of 3D printed fiber reinforced sustainable construction material, Mater. Lett. 209 (2017) 146–149, https://doi.org/10.1016/j.matlet.2017.07.123.
[20] B. Zareiyan, B. Khoshnevis, Effects of interlocking on interlayer adhesion and strength of structures in 3D printing of concrete, Autom. Constr. 83 (2017) 212–221, https://doi.org/10.1016/j.autcon.2017.08.019.
[21] A.P. Sheppard, R.M. Sok, H. Averdunk, Techniques for image enhancement and segmentation of tomographic images of porous materials, Phys. A 339 (2004) 145–151.